Proceedings of the 28th IEEE
EMBS Annual International Conference
New York City, USA, Aug 30-Sept 3, 2006

An Automatic Method for Ground Glass Opacity Nodule Detection and Segmentation from CT Studies

Jinghao Zhou, Sukmoon Chang, Dimitris N. Metaxas,
Binsheng Zhao, Michelle S. Ginsberg, and Lawrence H. Schwartz

Abstract— **Ground Glass Opacity (GGO) is de£ned as hazy increased attenuation within a lung that is not associated with obscured underlying vessels. Since pure (non-solid) or mixed (partially solid) GGO at the thin-section CT are more likely to be malignant than those with solid opacity, early detection and treatment of GGO can improve a prognosis of lung cancer. However, due to indistinct boundaries and inter- or intra-observer variation, consistent manual detection and segmentation of GGO have proved to be problematic. In this paper, we propose a novel method for automatic detection and segmentation of GGO from chest CT images. For GGO detection, we develop a classi£er by boosting k-Nearest Neighbor (k-NN), whose distance measure is the Euclidean distance between the nonparametric density estimates of two regions. The detected GGO region is then automatically segmented by analyzing the 3D texture likelihood map of the region. We applied our method to clinical chest CT volumes containing 10 GGO nodules. The proposed method detected all of the 10 nodules with only one false positive nodule. We also present the statistical validation of the proposed classi£er for automatic GGO detection as well as very promising results for automatic GGO segmentation. The proposed method provides a new powerful tool for automatic detection as well as accurate and reproducible segmentation of GGO.**

I. INTRODUCTION

Ground Glass Opacity (GGO) is de£ned as hazy increased attenuation within a lung that is not associated with obscured underlying vessels, but with preservation of bronchial and vascular margins [1]. It can re¤ect minimal thickening of the septal or alveolar interstitium, thickening of alveolar walls, or the presence of cells or ¤uid £lling the alveolar spaces. It can represent active disease such as pulmonary edema, pneumonia, or diffuse alveolar damage. The results of the Early Lung Cancer Action Project, or ELCAP, suggested that nodules with pure (non-solid) or mixed (partially solid) GGO at the thin-section CT are more likely to be malignant than are those with solid opacity [2]. A focal area of pure GGO on the thin-section CT seems to be an early sign of bronchoalveolar carcinoma (BAC) [3]. Pure GGO is useful for differentiating small localized BAC from small adenocarcinomas not having a replacement growth pattern [4]. Early detection and treatment of pure GGO can also improve a prognosis of lung cancer [5].

The appearances of GGO on CT images such as its shape, pattern, and boundary are very different from solid nodules. Thus, algorithms developed for segmentation of solid nodules are most likely to produce inaccurate results when applied to GGO. In [6], a hybrid neural network of three single nets and an expert rule are applied to detect GGO. This method underestimates GGO area due to its improper cut-off of the edges of GGO. Hence, this method may be used only for large GGO and may not be able to obtain accurate segmentation for small GGO. [7] detected GGO using automatic clustering techniques and focused only on GGO detection. The GGO segmentation was not discussed in their work. On the other hand, [8] proposed a GGO segmentation method based on Markov random £eld and vessel removal method based on shape analysis. However, they only focused on GGO segmentation. The GGO detection was not discussed in their work.

In this paper, we propose a novel method for automatic detection and segmentation of GGO from chest CT images. For GGO detection, we develop a classi£er by boosting k-Nearest Neighbor (k-NN), whose distance measure is the Euclidean distance between the nonparametric density estimates of two regions. The detected GGO region is then automatically segmented by analyzing the 3D texture likelihood map of the region. We also present the statistical validation of the proposed classi£er for automatic GGO detection as well as the very promising results of automatic GGO segmentation. The proposed method provides a new powerful tool for automatic detection as well as accurate and reproducible segmentation of GGO.

II. METHOD

A. GGO Detection

We £rst develop a novel method for automatic GGO detection from chest CT images. The method is based on 3D volume analysis using a machine learning framework, i.e., boosting a k-NN classi£er. Our primary focus in this section is the accurate classi£cation of GGO from other objects in chest CT images.

1) Vessel and Noise Suppression with 3D Cylinder Filters: The accuracy of GGO detection may be hindered by various structures within a lung. To avoid this dif£culty, we £rst develop a 3D cylinder £lter to suppress intensity values of

J. Zhou and D. Metaxas are with the Center for Computational Biomedicine Imaging and Modeling (CBIM), Department of Computer Science, Rutgers University, New Brunswick, NJ, USA jhzhou@eden.rutgers.edu, dnm@cs.rutgers.edu

S. Chang is with CBIM, Rutgers University and also with the Department of Computer Science, Capital College, Penn State University, Middletown, PA, USA sukmoon@psu.edu

B. Zhao is with the Departments of Medical Physics and Radiology, Memorial Sloan-Kettering Cancer Center, New York, NY, USA zhaob@mskcc.org

M. Ginsberg and L. Schwartz are with the Department of Radiology, Memorial Sloan-Kettering Cancer Center, New York, NY, USA ginsberm@mskcc.org, schwartl@mskcc.org

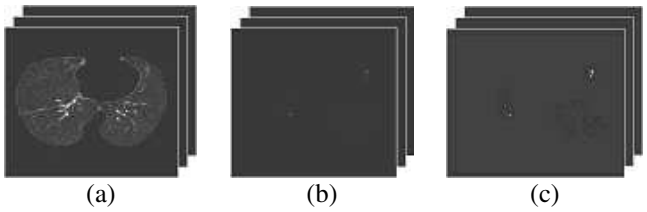

Fig. 1. Effect of F_{cyl}. (a) Original volume, (b) Volume £ltered with F_{cyl}, (c) After thresholding.

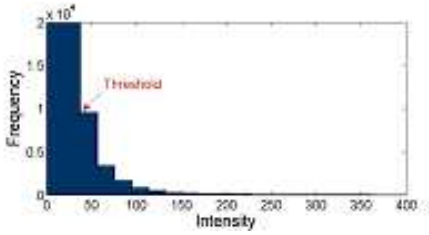

Fig. 2. Histogram of a cylinder £ltered volume.

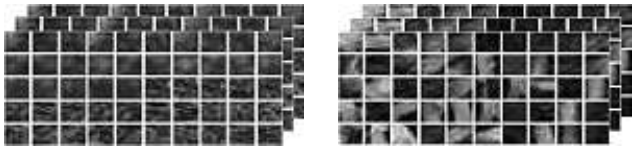

Fig. 3. Volumetric samples for learning. (a) Positive (GGO) samples, (b) Negative (non GGO) samples.

vessels and other elongated structures as well as noise inside a lung, while maintaining GGO intensity values intact [9]. The cylinder £lter F_{cyl} is de£ned as:

$$F_{\text{cyl}}(x) = \min_{\theta} \left(\min_{y \in \Omega_{\theta}^{x}} I(y) \right)$$

where, Ω_{θ}^{x} is the domain of the cylinder centered at x with orientation θ. F_{cyl} is a hybrid neighborhood proximity £lter that produces strong responses to blob-like objects (i.e. GGO). In this paper, we have selected the parameters of F_{cyl} empirically and used a cylinder with the radii of 1, 2 and 3 voxels and the length of 7 voxels at 7 different orientations. The effect of F_{cyl} is shown in Fig.1. In the £gure, (b) shows the £lter-response volume of F_{cyl} applied to (a). We can see from (b) that vessels and noise are effectively suppressed while GGO remains intact.

To isolate candidate GGO regions, i.e., regions of high response values, we apply a simple thresholding to the £lter-response volume (Fig.1(c)). The threshold value is automatically determined by analyzing the histogram of the £lter-response image, as illustrated in Fig.2. In the next section, we apply a machine learning framework to classify the candidate GGO regions.

2) Classi£cation of GGO by boosting k-NN: To apply supervised learning framework, we £rst collected volumetric samples of positive (GGO) and negative (non-GGO) instances, as shown in Fig.3. Let Ψ_M be the region of a volumetric sample bounded by a cube. We estimate the probability density function (pdf) of the intensity values of the interior of Ψ_M. We use a nonparametric kernel based method to approximate the pdf. Let i, $i = 0, \ldots, 255$, denote the random variable for intensity values. The intensity pdf of Ψ_M is de£ned by:

$$P(i|\Psi_M) = \frac{1}{V(\Psi_M)} \iiint_{\Psi_M} \frac{1}{\sqrt{2\pi\sigma^2}} \exp\left(-\frac{(i - I(y))^2}{2\sigma^2} \right) dy \quad (1)$$

where, $V(\Psi_M)$ denotes the volume of Ψ_M, y are the interior voxels of Ψ_M, and σ is the standard deviation of a Gaussian kernel. Fig.4 shows the typical intensity pdf of positive and negative instances. We can see from the £gure that positive and negative instances are well separable using the pdf. For this reason, we use as an instance the intensity pdf of the volumetric samples.

For the candidate GGO areas isolated as described in Sec. II-A, the learning for their classi£cation has a discrete target function of the form $f : \mathcal{R}^n \mapsto \mathcal{V}$, where $\mathcal{V} = \{\oplus, \ominus\}$, with the label $\oplus$ for GGO and $\ominus$ for non GGO areas. For k-NN, an instance x is represented as a point in n-dimensional space $\mathcal{R}^n$ by a feature vector $\langle a_1(x), a_2(x), \ldots, a_n(x) \rangle$, where $a_i(x) = P(i|\Psi_M)$. The standard Euclidean distance is used as the distance measure between two instance vectors. Given a query instance x_q to be classi£ed, k-NN returns $\hat{f}(x_q)$, as its estimate of $f(x_q)$, which is the most common value of f among the k training instances nearest to x_q:

$$\hat{f}(x_q) = \arg\max_{v \in \mathcal{V}} \sum_{i=1}^{k} \delta(v, f(x_i))$$

where, $x_1, \ldots, x_k$ denote the k instances from the training samples that are nearest to x_q, and $\delta(a, b) = 1$ if $a = b$ and $\delta(a, b) = 0$ otherwise. To obtain an accurate classi£cation, k-NN requires a large training set, which results in slow classi£cation due to the large number of distance calculations. We overcome this dif£culty by boosting k-NN [10]. As in [10], our purpose for boosting k-NN is to improve the speed of k-NN by reducing the number of prototype instances and thus reducing the required number of distance calculation without affecting the error rate. The details of boosting k-NN is given in [10]

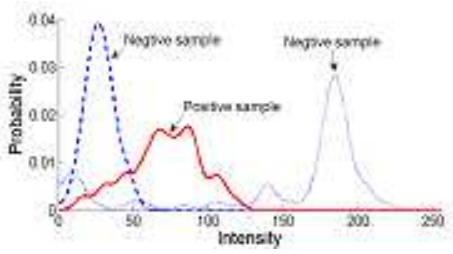

Fig. 4. Typical probability density functions of positive (solid line, GGO), negative (dash-dot line, typical background), and negative (dotted line, typical vessels) examples.

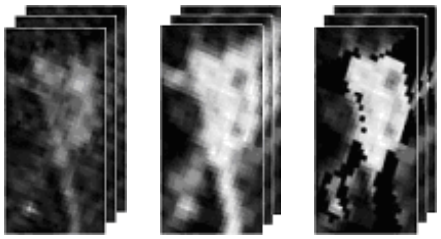

(a) (b) (c)

Fig. 5. GGO segmentation. (a) ROI containing a classi£ed GGO, (b) 3D likelihood map in ROI, (c) 3D likelihood map in ROI after vessel removal.

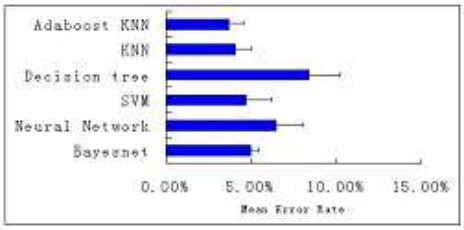

Fig. 6. Comparison of the mean error rates of various classi£ers by bootstrapping.

B. GGO Segmentation in ROI

Because of the hazy appearance of GGO and the large overlap of intensity values between GGO and surrounding vessels, simple thresholding or edge based segmentation methods do not produce acceptable results for GGO segmentation. The proposed method applies 3D texture likelihood map method using a nonparametric density estimation for segmentation [11], followed by eigenanalysis of the Hessian matrix to accurately remove vessels overlapped with GGO [12], [13].

1) 3D Texture Likelihood Map Using Nonparametric Density Estimation: We £rst extract the ROI (Region Of Interest) surrounding a classi£ed GGO. For each voxel in the ROI, we evaluate the likelihood of the voxel belonging to GGO by measuring 3D texture consistency between the GGO and a small spherical region (i.e., 3D texon) centered at the voxel.

Let Φ_M be the region of a volumetric sample of a classi£ed GGO bounded by a sphere. Using Eq.1, we estimate the pdf of the intensity values of the interior of Φ_M, that is, $p_{_M} = P(i|\Phi_M)$. Similarly, let Φ_T be the region of the 3D texon centered at the given voxel in the ROI. Using Eq.1, we also estimate the pdf of the intensity values of the interior of Φ_T, that is, $p_{_T} = P(i|\Phi_T)$. To measure the dissimilarity between the two pdfs, we use an information theoretic distance measure called Kullback-Leibler Divergence (KLD) [14]. The Bhattacharya distance, which is a symmetrized variation of KLD, between p_M and p_T is:

$$\begin{aligned} B(p_{_M}\|p_{_T}) &= -\log \rho(p_{_M}\|p_{_T}) \\ &= -\log \int [p_{_M}(i)]^{\frac{1}{2}}\,[p_{_T}(i)]^{\frac{1}{2}}\,di. \end{aligned}$$

We now evaluate the 3D texture likelihood of the 3D texon at every voxel in ROI. We de£ne this likelihood using ρ, since it increases as the Bhattacharya distance between two distributions decreases. Fig.5(b) shows the 3D texture likelihood map of the volume in (a). The radius of 3D texons used in our paper is 3 pixels and the model interior texture is mostly homogeneous with some level noise. Thus, it is not necessary to consider the spatial correlation between pixels.

2) Vessel Removal: Finally, we remove the vessels around GGO in the 3D texture likelihood map. The eigenanalysis of the Hessian matrix is a widely used method for vessel detection [12], [13]. Given an image $I(x)$, the local intensity variations in the neighborhood of a point x_0 can be expressed with its Taylor expansion:

$$I(x_0 + h) \approx I(x_0) + h^T \nabla I(x_0) + h^T H(x_0) h$$

where, $\nabla I(x_0)$ and $H(x_0)$ denote the gradient and the Hessian matrix at x_0, respectively. $H(x_0)$, whose components are the second order derivatives, describes the curvature of $I(x)$ at x_0. Let $\lambda_1, \lambda_2, \lambda_3$ and $\vec{e_1}, \vec{e_2}, \vec{e_3}$ be the eigenvalues and eigenvectors of H such that $\lambda_1 \leq \lambda_2 \leq \lambda_3$ and $|\vec{e_i}| = 1$. The signs and ratios of the eigenvalues provide the indications of various shapes of interest, as summarized in Table I. Fig.5(c) shows the texture likelihood map after the removal of vessels in (b).

III. RESULTS

To test the GGO detection method, we collected 600 volumetric samples, containing 400 training samples and 200 testing samples. The samples were of size $9 \times 9 \times 3$ voxels extracted from the CT volumes. Each sample was converted to an instance vector in $\mathcal{R}^{256}$, representing its nonparametric density estimate. For the boosted k-NN, we used the standard Euclidean distance as the distance measure between two instances as described in Sec. II-A. We performed bootstrapping to estimate the generalization error of our GGO detection method [15]. We trained and tested the proposed method on bootstrap samples. After 20 steps of boosting, the test error rate converged to 3.70%.

We also compared the boosted k-NN (20 boosting steps with $k = 3$) to other classi£ers, i.e., k-NN classi£er ($k = 3$), decision tree, support vector machine, neural network (1 hidden layer, learning rate of 0.3), and Bayes network. Fig.6 summarizes the results. The multiple comparison test ($p = 0.05$) shows that the boosted k-NN and k-NN are signi£cantly superior to other classi£ers. Note that, although our purpose for boosting k-NN was not to improve the classi£cation accuarcy but rather to speed up the classi£cation process, the results show that boosting k-NN also improves the classi£cation accuracy over k-NN.

TABLE I

CRITERIA FOR EIGENVALUES AND CORRESPONDING SHAPES.

Eigenvalues	Shape
$\lambda_1 \leq 0, \lambda_2 \leq 0, \lambda_3 \leq 0$	blob
$\lambda_1 \leq 0, \lambda_2 \leq 0, \lambda_3 \approx 0$	tube
$\lambda_1 \leq 0, \lambda_2 \approx 0, \lambda_3 \approx 0$	plane
$\lambda_1 \leq 0, \lambda_2 \leq 0, \lambda_3 \geq 0$	double cone

We applied the trained GGO classi£er to 10 CT volumes containing 10 nodules. The CT volumes were acquired by multi-slice HRCT scanners with 1 mm slice collimation. The number of slices in each CT scan ranged from 23 to 29 (interpolated to 92 to 116), each of which consists of a 512×512 pixels, with in-plane resolution ranging from 0.57mm to 0.71mm. The classi£er detected the total of 11 nodules, containing all of the 10 nodules and one false positive nodule.

The detected nodules were then segmented as described in Sec. II-B. Fig.7 shows the GGO segmentation results overlaid on the original CT images and 3D reconstruction for four GGOs as examples. From the £gure, we can see that the surrounding vessels are accurately removed from the GGO segmentation. These results demonstrate the potential of our segmentation method to deal with haze patterns of GGO.

IV. CONCLUSION

We proposed a novel method for the automatic detection and segmentation of GGO from chest CT images. The proposed method consists of two steps, i.e., GGO detection, followed by GGO segmentation. For GGO detection, vessels and noise were £rst suppressed using 3D cylinder £lters. Then, candidate GGO regions were extracted by thresholding. We automatically selected the threshold by the intensity histogram analysis of the £lter-response volumes. Finally, the candidate GGO regions were classi£ed by boosting k-NN, whose distance measure was the Euclidean distance between the intensity probability density functions of two examples. The validation of the proposed method using bootstrapping shows the mean error rate of 3.70%. Our method applied to clinical chest CT volumes containing 10 GGO nodules also showed the promissing results, detecting all of the 10 nodules with one false positive nodule.

Each GGO region classi£ed was then automatically segmented by analyzing the 3D texture likelihood map of the region. We presented various results of GGO detection and segmentation from clinical chest CT images. The manual segmentation of GGO has proved to be problematic due to large inter-observer variations as well as intra-observer variations. The proposed method introduces a novel automatic tool for accurate detection as well as accurate and reproducible segmentation of GGO.

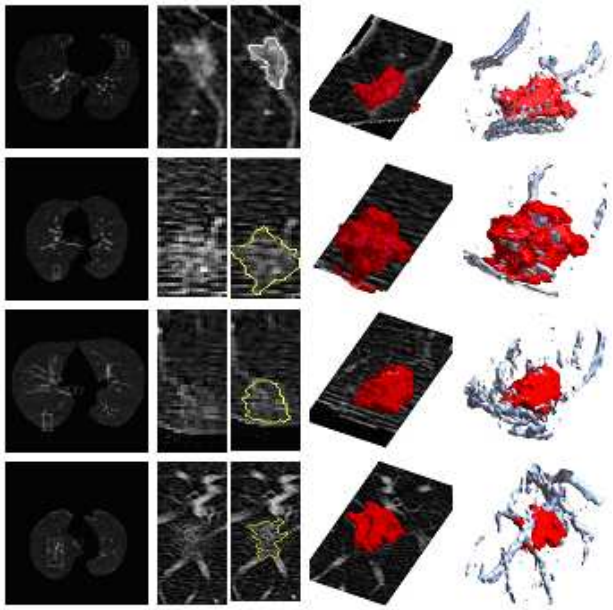

Fig. 7. GGO segmentation—four segmented GGO nodules are shown. (a) original CT images containing GGO nodules, (b) enlarged GGO areas, (c) segmented GGO, (d) 3D reconstruction of segmented GGO overlaid with original CT images in (a), and (e) 3D reconstruction of segmented GGO with other nearby structures.

REFERENCES

[1] J. Austin, N. Muller, and P. e. a. Friedman, "Glossary of terms for CT of the lung: recommendations of the nomenclature committee of the ¤eischner society," *Radiology*, vol. 200, pp. 327–331, 1996.

[2] C. Henschke, D. Yankelevitz, and R. Mirtcheva, "CT screening for lung cancer: frequency and signi£cance of part-solid and nonsolid nodules," *Am. J. Roentgenol.*, vol. 178, pp. 1053–1057, 2002.

[3] H. Jang, K. Lee, O. Kwon, C. Rhee, Y. Shim, and J. Han, "Bronchioloalveolar carcinoma: focal area of ground-glass attenuation at thin-section CT as an early sign," *Radiology*, vol. 199, pp. 485–488, 1996.

[4] K. Kuriyama, M. Seto, T. Kasugai, M. Higashiyama, S. Kido, Y. Sawai, K. Kodama, and D. Kuroda, "Ground-glass opacity on thin-section CT: value in differentiating subtypes of adenocarcinoma of the lung," *Am. J. Roentgenol.*, vol. 173, pp. 465–469, 1999.

[5] S. Watanabe, T. Watanabe, K. Arai, T. Kasai, J. Haratake, and H. Urayama, "Results of wedge resection for focal bronchioloalveolar carcinoma showing pure ground-glass attenuation on computed tomography," *Ann. Thorac. Surg.*, vol. 73, pp. 1071–1075, 2002.

[6] K. Heitmann, H.-U. Kauczor, P. Mildenberger, T. Uthmann, J. Perl, and M. Thelen, "Automatic detection of ground glass opacities on lung HRCT using multiple neural networks," *European Radiology*, vol. 7, pp. 1463–1472, 1997.

[7] M. Tanino, H. Takizawa, S. Yamamoto, T. Matsumoto, Y. Tateno, and T. Iinuma, "A detection method of ground glass opacities in chest x-ray CT images using automatic clustering techniques," in *SPIE*, vol. 5032, 2003, pp. 1728–1737.

[8] L. Zhang, M. Fang, D. Naidich, and C. Novak, "Consistent interactive segmentation of pulmonary ground glass nodules identi£ed in CT studies," in *SPIE*, vol. 5370, 2004, pp. 1709–1719.

[9] S. Chang, H. Emoto, D. Metaxas, and L. Axel, "Pulmonary micronodule detection from 3d chest CT," in *MICCAI*, 2004, pp. 821–828.

[10] Y. Freund and R. Schapire, "Experiments with a new boosting algorithm," in *the* 13^{th} *International Conference on Machine Learning*, 1996, pp. 148–156.

[11] X. Huang, Z. Qian, R. Huang, and D. Metaxas, "Deformable-model based textured object segmentation," in *EMMCVPR*, 2005, pp. 119–135.

[12] P.-E. Danielsson and Q. Lin, "Ef£cient detection of second-degree variations in 2d and 3d images," *Journal of Visual Communication and Image Representation*, vol. 12, pp. 255–305, 2001.

[13] C. Lorenz, I.-C. Carlsen, T. Buzug, C. Fassnacht, and J. Weese, "Multi-scale line segmentation with automatic estimation of width, contrast and tangential direction in 2d and 3d medical images," in *CVRMed-MRCAS*, 1997, pp. 233–42.

[14] S. Ali and S. Silvey, "A general class of coef£cients of divergence of one distribution from another," *J. Roy. Stat. Soc.*, vol. 28, pp. 131–142, 1966.

[15] B. Efron, "Estimating the error rate of a prediction rule: Improvement on cross-validation," *Journal of the American Statistical Association*, vol. 78, pp. 316–331, 1983.